Hydrophilic Silver Nanoparticles for Hg(II) Detection in Water: Direct Evidence for Mercury−Silver Interaction

Irene Schiesaro,[$] Luca Burratti,[$] Carlo Meneghini, Ilaria Fratoddi, Paolo Prosposito, Joohyun Lim, Christina Scheu, Iole Venditti, Giovanna Iucci, and Chiara Battocchio*
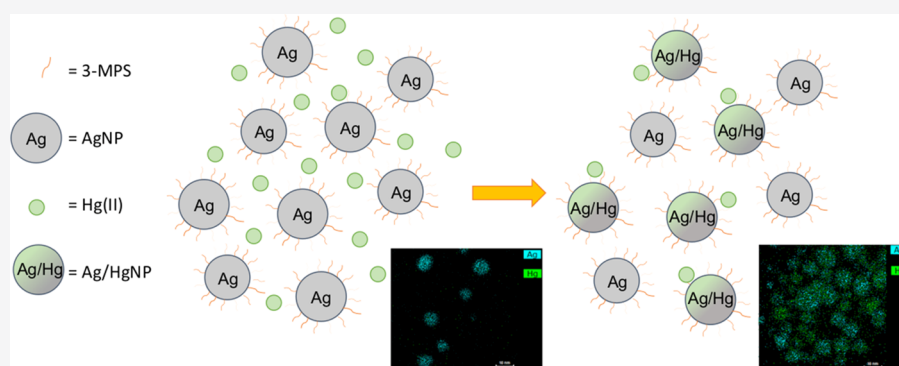
ACCESS | Metrics & More | Article Recommendations | SI Supporting Information

ABSTRACT: In this work, the electronic and molecular structure, as well as the morphology, of innovative nanostructured materials whose optical properties respond to the presence of heavy metals in water samples was investigated. In particular, the here discussed silver nanoparticles (NPs) stabilized by a hydrophilic ligand (sodium 3-mercapto-1-propanesulfonate, 3MPS) are able to reveal the presence of mercury ions at ppm levels. The sensitivity of the proposed nanosensor to Hg(II) in 1−5 ppm range was ascertained by optical tests; then, the local chemistry and electronic structure of the nanostructured coordination compounds made of functionalized silver nanoparticles (NPs) and metal ions, and their correlation with the resulting nanoaggregates' shape and morphology, were investigated by state-of-the-art synchrotron radiation (SR)-induced spectroscopies and transmission electron microscopy (TEM). In particular, SR-induced X-ray photoelectron spectroscopy (XPS) and X-ray absorption spectroscopy (XAS) measurements allowed us to gather complementary information about the silver−mercury interaction, which is only partially mediated by the negatively charged 3MPS ligand, different from what was observed for analogous nanosensors applied to other bivalent heavy metal ions, for example, Co(II) and Ni(II). TEM morphological analysis sheds light on the structure of the AgNP-3MPS/Hg aggregates, revealing the formation of Ag/Hg alloy nanoparticles.

INTRODUCTION

Monitoring the levels of heavy metal ions such as Co(II), Ni(II), Cu(II), and Hg(II) in aquatic ecosystems is important because these ions can have severe effects on the health of humans and animals.[1,2]

In the last decade, many efforts have been devoted to developing devices and technologies to detect and monitor heavy metals in water, and nanomaterials are promising systems in this regard.[3−7]

Among others, Hg-based pollutants that arise mainly from coal-burning power plants are of great environmental concern because of the high toxicity of many Hg compounds. Hg(II) is one of the most toxic metal ions and damages various human organs, resulting in serious symptoms and health deterioration. Therefore, the fabrication of sensitive and selective methods to monitor the presence of such heavy metal ions is of great significance to protect public health and the environment.[8,9] The traditional procedures for the detection of such ions in

water employ high-performance liquid chromatography (HPLC), atomic fluorescence spectroscopy (AFS), flame atomic absorption spectroscopy (FAAS), and graphite furnace atomic absorption spectroscopy (GFAAS).[10,11] Although these methods offer high sensitivity and accuracy in metal ion detection and determination, they are time-consuming, costly, and/or require sophisticated instruments. To circumvent these problems, nanomaterial (mainly gold and silver nanoparticles (NPs))-based sensors have evolved, incorporating massive sensing-based techniques to provide simple, low-cost, and

rapid tracking of heavy metals in real samples.[12] The methods of determination rely on the unique size and interparticle distance-dependent absorption spectra and color change of the nanoparticle-containing solution; the wavelength of the SPR peak strongly depends on the particle composition, dimension, shape, and chemical functionalization.[13,14]

In this framework, the possibility to design and synthesize hydrophilic noble metal nanoparticles of precisely tunable and controlled dimensions that are able to capture and coordinate heavy metal ions is an appealing perspective attracting many research efforts.[15−20] Among other noble metals, silver nanoparticles are the best-suited candidates for plasmonic detection of analytes;[21] indeed, it was recently demonstrated that AgNPs yield a rapid localized surface plasmon resonance response compared to AuNPs with augmented sensitivity.[22]

Measurements carried out using synchrotron radiation (SR)-X-ray photoelectron spectroscopy (XPS) and ultraviolet (UV)−visible absorption spectroscopy on AgNPs functionalized by negatively charged thiol 3-mercapto-1-propanesulfonate (3MPS) allowed us to assess the ability of such nanoparticles to coordinate Co(II) and Ni(II) ions.[23] Moreover, TEM analysis revealed that Co^{2+} and Ni^{2+} are able to induce different shapes in the AgNP-heavy-metal aggregates; this finding was also supported by theoretical simulations.[24] Some authors observed that AgNPs stabilized with citrate can be oxidized by traces of Hg(II), producing Ag(I) and Ag/Hg amalgam.[16,25] This would suggest that the AgNP−Hg(II) interaction mechanism, which leads to the silver nanoparticle optical response to mercury ions present in water, is completely different from the one observed for other bivalent cations, such as Co(II) and Ni(II).[26]

In this work, we focus our attention on the determination of the local coordination chemistry, atomic structure, and electronic structure of the AgNP-3MPS/Hg system. Thereby, the AgNP-3MPS have mean diameters ranging from 3 to 8 nm and are tuned by the synthesis. Particular attention is devoted to probing the Ag/Hg interaction. Due to the complexity of the nanostructured adducts, complementary characterization techniques were applied to obtain a most complete and accurate description of the electronic structure, local coordination geometry, and molecular stability of the AgNP-3MPS/Hg(II) nanoaggregates. In this context, we probed the electronic structure and coordination chemistry of the heavy metal by SR-XPS and the local structure around the silver nanoparticles with X-ray absorption spectroscopy (XAS) measurements using the Ag K-edge and Hg L_{III}-edge. TEM analysis and elemental maps have been used to check carefully the modifications occurring in the nanoparticle morphology upon interaction with Hg(II). In a previous study, SR-XPS, XAS, and TEM results were successfully combined by some authors for the description of AgNPs stabilized by allylmercaptane (AM) thiols.[27] At that time, the three complementary techniques coherently suggested a core−shell system in which a metallic (Ag) core is surrounded by a Ag_2S-like shell, the thickness being a function of the synthesis route and a layer of sulfur ions bridging the thiol chains to the Ag atoms of the NP surface. Here, we expect that the combined SR-XPS, XAS, and TEM investigation allows us to ascertain the silver nanoparticle stability and 3MPS molecular integrity upon interaction with mercury ions, as well as to shed light on the AgNP−Hg interaction mode.

This information is required to design a suitable route for the synthesis of nanomaterial-based sensors aimed at providing simple, low-cost, and rapid tracking of heavy metals in real samples in the main framework of protection and preservation of aquatic ecosystems.

■ MATERIALS AND METHODS

Synthesis of AgNP-3MPS + Hg(II). Silver nitrate $(AgNO_3)$, sodium borohydride $(NaBH_4)$, and 3MPS were purchased from Sigma Aldrich, while mercury nitrate monohydrate $[Hg(NO_3)_2·H_2O]$ was purchased from Agros Organics. All of the reagents were used without further purification. Deionized water (electrical conductivity 18 $\mu\Omega$/cm at room temperature) obtained from a Millipore Milli-Q water purification system was used for the preparation of the colloidal aqueous solutions.

The silver nanoparticles stabilized with 3MPS were synthesized according to a previous study.[28] Briefly, a volume of 700 mL of sodium borohydride water solution (4 mM) at T = 3 °C was subject to vigorous stirring. Next, 10 mL of this solution was used to solubilize 0.2 g of 3MPS (capping agent solution). A volume of 46 mL of $AgNO_3$ water solution (2 mM) was added dropwise to the remaining solution (690 mL), while a small volume of the capping agent solution (84.3 μL) was introduced at the end of the synthesis. A washing procedure was not applied.

Finally, the colloidal solution was refrigerated at T = 4 °C before being used for contamination with Hg(II).

The procedure to prepare AgNP-3MPS/Hg(II) nanoaggregates is reported in detail in a previous study.[26] Briefly, a fixed volume of AgNP water solution was added to the same volume of a water solution containing the heavy metal ions at a specific concentration (1 and 5 ppm). To obtain the final powder samples, the solutions were dried in an oven at T = 50 °C under continuous gentle stirring, and the powders were used for SR-XPS and XAFS analyses. To prevent degradation of the samples, the dry powders of the reference (AgNP-3MPS) and AgNP-3MPS/Hg(II) nanoaggregates were stored under vacuum at room temperature until measurements were conducted.

Spectroscopic and Microscopic Techniques. *Synchrotron Radiation (SR)-Induced X-ray Photoelectron Spectroscopy (SR-XPS).* Experiments were carried out at the Materials Science Beamline (MSB) at the Elettra synchrotron radiation source (Trieste, Italy). MSB is placed at the left end of the bending magnet 6.1, and it is equipped with a plane-grating monochromator that provides light in the energy range of 21−1000 eV. The base pressure in the UHV end-station is 2 × 10^{-10} mbar. The end-station is equipped with a SPECS PHOIBOS 150 hemispherical electron analyzer, low-energy electron diffraction optics, a dual-anode Mg/Al X-ray source, an ion gun, and a sample manipulator with a K-type thermocouple attached to the rear side of the sample.

Photoelectrons emitted by C 1s, O 1s, S 2p, Ag 3d, N 1s, and Hg 4f core levels at normal emission geometry were collected. For all signals except S 2p, photon energy of 630 eV impinging at 60° was selected. Since the S 2p signal intensity was very low due to element dilution, photon energy of 350 eV was selected to measure this core level. The spectral resolution for this experiment was 0.60 eV. Spectra binding energy (BE) calibration was performed using the aliphatic C 1s, always found at 285.0 eV BE,[29] as the internal reference. As a baseline, we used a cubic spline; Gaussian peak functions were chosen as signal components to fit the photoelectron spectra.[30] S $2p_{3/2,1/2}$, Ag $3d_{5/2,3/2}$, and Hg $4f_{7/2,5/2}$ doublets were fitted

using the same full width at half-maximum (FWHM) for both spin−orbit components: a spin−orbit splitting of 1.2, 6.0, and 4.1 eV, respectively, and branching ratios $2p_{3/2}/2p_{1/2}$ = 2/1, $3d_{5/2}/3d_{3/2}$ = 3/2, and $4f_{7/2}/4f_{5/2}$ = 4/3.

X-ray Absorption (XAS). The experiment was performed at the XAFS beamline of Elettra (Italy).[31] Spectra were collected at room temperature in transmission geometry at the K-edge of Ag (E_{Ag} = 25 514 eV) and in fluorescence geometry for the L_{III} edge of Hg (E_{Hg} = 12 284 eV). To obtain statistical reliability, several spectra were acquired and averaged for each sample. The extended X-ray absorption fine structure (EXAFS) signal χ^{exp} was extracted from the raw absorption spectra using the ESTRA program[32] following the standard procedure consisting of linear pre-edge subtraction and postedge normalization. Quantitative XAFS data analysis was performed using the program FitEXA[32] fitting through a least-squares procedure the k-weighted EXAFS signal $k\chi^{exp}$ with a theoretical model $k\chi^{th}$ (where k is the photoelectron wavenumber $k = \hbar^{-1}\sqrt{2m_e\Delta E}$; m_e is the electron mass and $\Delta E = E - E_0$ is the photoelectron energy, which is the difference between the X-ray energy E and the absorption edge energy E_0). The theoretical curve was modeled as a sum of partial contributions using the standard EXAFS formula[33] with Gaussian disorder approximation. Each contribution is assumed to be Gaussian-shaped at an average neighbor distance R_i with multiplicity number N_i and mean square relative displacement (MSRD) σ_i, which were obtained via the refinement procedure. The amplitude, phase, and mean free path function required for the theoretical model were calculated using the FEFF8.2 program[34] for the atomic clusters generated on the basis of the selected crystallographic structures.

High-Resolution Transmission Electron Microscopy (HRTEM). High-resolution transmission electron microscopy (HRTEM) was used to analyze the morphology, size, and shape of AgNP-3MPS before and after Hg(II) contamination at a concentration of 1 ppm. The HRTEM characterization of these samples was carried out in a transmission electron microscope equipped with an image corrector (FEI Titan Themis 60-300 X-FEG) operated at 300 kV. TEM images were recorded with 4k × 4k pixels on a metal−oxide−semi-conductor (CMOS) camera. High-angle annular dark-field scanning transmission electron microscopy (HAADF-STEM) was performed using two FEI 60-300 Titan Themis instruments operated at 300 kV with a Cs-corrector either for the image- or probe-forming lens. The chemical composition of AgNPs was confirmed by energy-dispersive X-ray spectroscopy (EDS) in the STEM mode using a Bruker X-EDS detector. For EDS maps, we used S-Kα, Ag-Lα, and Hg-Lα lines. Size analysis was carried out using the free software ImageJ on several TEM images for both samples AgNP-3MPS and AgNP-3MPS/Hg(II) at a concentration of 1 ppm.

The AgNP hydrodynamic mean diameter and size distribution were measured with a dynamic light scattering (DLS) instrument (Malvern Nano ZS90) at 25 °C in deionized water (18.3 MΩ·cm) obtained using a Zeneer Power I Scholar-UV instrument.

Optical Characterizations. *UV−Visible Absorption Spectroscopy.* The optical absorption spectra of the colloidal solutions of AgNP-3MPS and AgNP-3MPS/Hg(II) at different concentrations were collected in the range of 300−700 nm (UV−vis) using plastic cuvettes in a PerkinElmer spectrophotometer (Lamba19 UV/Vis/NIR). The AgNP-3MPS water

solution was mixed with different concentrations of Hg(II) water solution, and after 5 min of interaction, the absorption spectrum was recorded.

■ RESULTS AND DISCUSSION

Structural Investigation. SR-XPS experiments aimed at investigating the interaction between AgNPs and Hg(II) ions. C 1s, O 1s, Ag 3d, S 2p, and Hg 4f core level spectra were collected on AgNPs stabilized by 3MPS and treated with 1 and 5 ppm Hg(II) and analyzed by applying a peak-fitting procedure, as explained in the Materials and Methods section (all BE (eV), FWHM (eV), relative intensity values, and proposed signal assignments are reported in Table S1 in the Supporting Information file). The individuated spectral components confirm for both samples the stability of AgNPs and the capping efficiency of the 3MPS stabilizing agent, in agreement with already published data.[23,26] C 1s spectra can be fitted with two main components at 285.0 and 286.2 eV, respectively, assigned to C−C and C−S groups and three more components of lower intensity due to contamination, which is always found in samples prepared in aqueous solution and dried in air (288.3 eV C=O, 289.8 eV COOH, 291.0 eV COO⁻ functional groups). The O 1s spectra also show the presence of four different kinds of oxygen atoms in order of increasing BE as follows: the TiO_2 substrate (530.0 eV), S=O groups of sulfonate and C=O contaminants (532.1 eV), S−O⁻ sulfonate signal plus C−O groups of contaminants (533.3 eV), and physisorbed water (a small contribution at about 534.5 eV BE). The atomic ratio between S=O and S−O⁻-like signals is S=O/S−O⁻ = 2:1 for the sample with 1 ppm Hg(II) and S=O/S−O⁻ = 3:1 for the sample with 5 ppm Hg(II), very close to the theoretical ratio for the 3MPS moiety (S=O/S−O⁻ = 2:1). The small discrepancy in the 5 ppm Hg(II) sample is attributed to the contributions from contaminant carbonyl groups. Indeed, even if contaminant species affect the carbonyl signal intensity, the contamination is expected to affect all samples in a similar way, and the trend observed for the atomic ratios is indicative of the chemical stability of sulfonate groups. The C 1s and O 1s curve-fitting results (also reported in Figure S1 in the Supporting Information) confirm the stability of the 3MPS ligand on the surface of silver nanoparticles; however, it is common knowledge in the literature that the most indicative signals for the surface-structure analysis of metal nanoparticles stabilized by thiols are the metal (Ag 3d) and S 2p core levels. Indeed, Ag 3d and S 2p spectra of AgNP-3MPS treated with Hg(II) 1 ppm are provided in Figure 1 (and they are representative for both samples) and accurately discussed in the following section.

Ag 3d spectra (Figure 1a) are asymmetric at high BEs, a common feature in capped nanoparticles,[16,23] suggesting that the nanoparticle is composed of at least two different kinds of Ag atoms. The spin−orbit pair at lower BEs (Ag $3d_{5/2}$ = 368.09 eV BE) is attributed to metallic silver atoms of the nanoparticle core; the very small signal at a higher BE is usually associated with positively charged silver atoms at the NP surface interacting with the 3MPS ligand.[16,23]

S 2p spectra (Figure 1b) are, as expected for the 3MPS moiety, extremely complicated, showing two groups of components. The first large signal at around 162 eV is composited by at least two spin−orbit pairs, both indicative for sulfur atoms covalently bonded to silver but with two different hybridizations. The peaks at a lower BE (S $2p_{3/2}$ component at 160.4 eV BE) are attributed to S−Ag bonds with sp hybridized
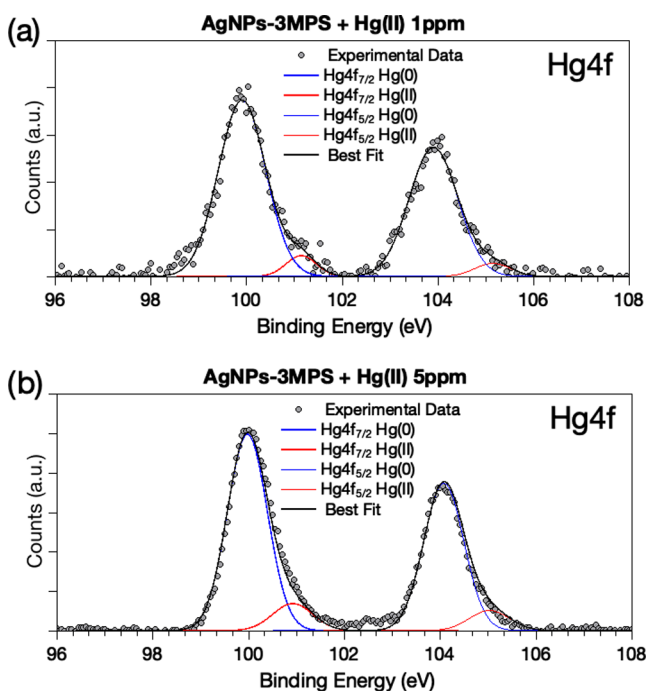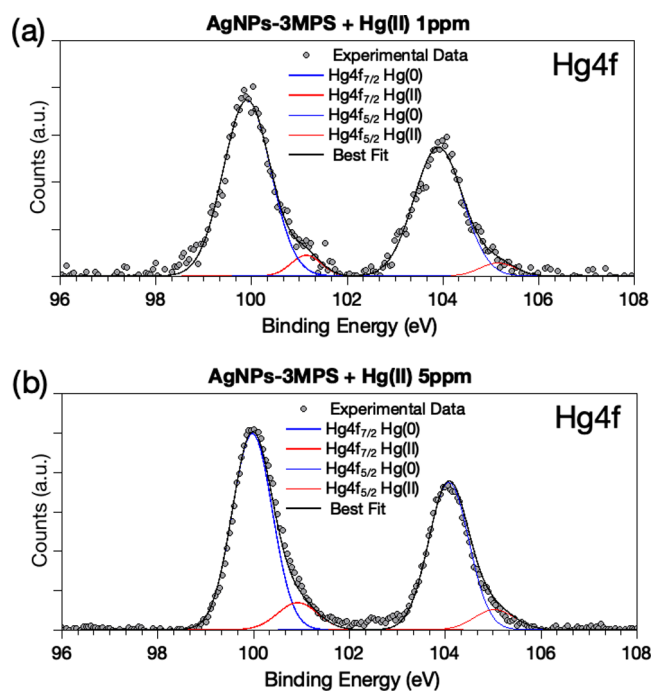
Figure 1. SR-XPS Ag 3d (a) and S 2p (b) spectra of AgNP-3MPS treated with Hg(II) 1 ppm.

Figure 2. SR-XPS Hg 4f spectra of (a) AgNP-3MPS treated with Hg(II) 1 ppm and (b) AgNP-3MPS treated with Hg(II) 5 ppm.

sulfur, and the signal at a higher BE (S $2p_{3/2}$ = 161.7 eV) suggests S−Ag bonds with S atoms hybridized in sp^3 configuration.[35,36] It is noteworthy that no physisorbed thiol moieties appear (R-SH S $2p_{3/2}$ signals are expected at around 163−164 eV BE), which is different from analogous systems[26] and is probably due to the slightly modified synthesis procedure, as described in the Materials and Method section. The two pairs of components at higher BE values (168.6 and 170.2 eV BE for the S $2p_{3/2}$ components) are due to the sulfonate moiety of 3MPS, as already discussed for analogous systems in the literature.[16,23,35]

SR-XPS measurements carried out at the Hg 4f core level allowed us to reveal Hg(II) presence in both samples and to probe the interaction between mercury and AgNP-3MPS. The Hg 4f spectra are shown in Figure 2a (AgNP-3MPS + 1 ppm Hg(II)) and Figure 2b (5 ppm Hg(II)).

It is noteworthy that in both samples, the Hg 4f spectra are clearly asymmetric, leading to two individuate pairs of spin−orbit components. The main component (Hg $4f_{7/2}$ BE = 99.9 eV) is consistent with Hg(0) atoms, as, for example, in amalgams;[37] the signal of lower intensity (around 10% of the whole Hg 4f signal) at a higher BE (about 101 eV) can be attributed to Hg(II) ions in oxides or coordination compounds in accordance with the literature.[38] This behavior is not surprising for Hg(II) ions interacting with silver nanoparticles; indeed, although other heavy metals, such as Ni(II) and Co(II), interact with silver nanoparticles by coordinating them through the ligands, giving rise to complex agglomerates with different shapes induced by the metals,[23,24,26] Hg(II) ions tend to react with silver atoms at the NP surface giving rise to Hg/Ag alloys.[16,25] In the literature, it is suggested that such an interaction could lead either to the formation of core−shell nanoparticles with a metallic silver core surrounded by a shell of AgHg alloy[39] or to smaller AgNPs. The latter are formed due to the dissolution of silver ions produced by a redox process in which Hg(II) oxidizes silver atoms to Ag(I),[40]

altering not only the chemical composition but also the morphology of the pristine AgNPs. However, since the Ag(I) ion XPS signal is expected at 368.00 eV BE (Ag $3d_{5/2}$),[27,41] a BE value that is very close to 368.09 BE individuated for Ag $3d_{5/2}$ component of Ag(0) atoms at the NP bulk, a BE shift related to Ag(I) formation leads to a Ag(0)−Ag(I) peak separation too small to be appreciated within the spectral resolution (0.60 eV). The local structure (XAS) and morphological (HRTEM) investigation reported in the following section is of primary importance to shed light on this point.

Looking at the k-weighted Ag K-edge EXAFS signal, reported in Figure 3, it is evident that in the region 5−14 Å^{-1} the structural signal is definitively weaker in the AgNP-3MPS sample treated with Hg(II) 5 ppm with respect to the data of the 1 ppm sample; moreover, the 5 ppm spectrum depicts evident oscillations in the k >14 Å^{-1} region, while the 1 ppm spectrum depicts quite an averagely flat spectrum and higher noise in this region. These features are likely ascribed to the presence of Hg neighbors, consistent with XPS data analysis results. In particular, the increasing structural signal in the k > 14 Å^{-1} region (5 ppm) is consistent with Ag−Hg correlations because the backscattering amplitude of Hg, being a high Z atom, increases at high k values. We show (see below) that the antiphase between Ag−Ag and Ag−Hg contribution is responsible for the attenuation of the structural EXAFS signal in the 5 ppm spectrum with respect to the 1 ppm spectrum. In the 1 ppm data, the contribution from Ag−Hg is weak, suggesting less contribution of Hg coordination around Ag in the 1 ppm sample.

The quantitative EXAFS data analysis was carried out following the procedure described in ref 27, and the best fits of the Ag K-edge EXAFS signal are reported in Figure 3. The model involves Ag in different coordination phases: the Ag metal fcc phase (Ag^{bulk}) representing the core of the NP, the Ag$_2$ S-like phase representing the contribution of Ag ions at the
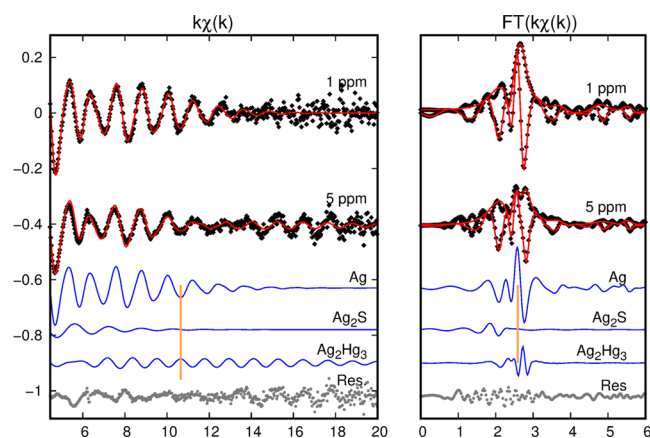
Figure 3. Ag K-edge results of AgNPs 1 ppm and 5 ppm. Experimental (black dots) and fit (red curves) results are presented together with the contribution involved in the analysis (5 ppm) and the residual (experimental best fit) shifted vertically for the sake of clarity. In the right panel, the moduli (|FT|) and imaginary parts (I-FT) of the Fourier transform (FT) of experimental (dots) and best fit (red curves) results are reported. The I-FT of partial contributions and residual and the orange vertical line points out the antiphase effect between Ag−Ag and Ag−Hg contributions in the 5 ppm data.

surface, and the Ag_2Hg_3 phase (amalgam), which takes into account the contribution of Ag atoms bound to Hg. Due to the large number of parameters involved, many of them have been constrained, taking into account the coordination chemistry of model compounds. Along the lines described in ref 27, we assumed a fraction x of Ag in Ag^{bulk}, a fraction y in Ag_2S, and a fraction z in Ag_2Hg_3 (where x + y + z = 1). The Ag^{bulk} phase includes four contributions whose distances have been constrained to the face-centered cubic (fcc) crystallographic structures. As single free parameters, the first shell distance R_{AgAg} was used while the coordination number was calculated with the formula $xN_i^{bulk}(1 - pR_i)$, where N_i^{bulk} is the Ag coordination of the i-th shell in Ag^{bulk} and the term in parentheses takes into account the reduction of effective coordination due to the finite size of the NP.[27] To model the Acantite-like phase, two shells are considered: $R_{AgS}^{Ag_2S}$ at 2.5 Å and $R_{AgAg}^{Ag_2S}$ at 3.2 Å. On extending the fit up to 20 Å^{-1} in the k space, the contributions from the two phases are not sufficient to obtain a good fit, but adding the path to R_{AgHg} (Å) at 2.89 Å expected from the Ag_2Hg_3 phase considerably improves the fit.

In Figure 3, the best fits (red curves) for the 1 and 5 ppm sample experimental data (black dots) are reported and the calculated contributions of the three phases involved (5 ppm sample) are presented (blue curves), along with the residual (experimental best fit) vertically shifted for the sake of clarity.

It is noticeable that AgM and Ag_2S oscillations are damped at high k, while oscillations of Ag_2Hg_3 reproduce well the experimental data.

Looking at the R space in the right panel of Figure 3, it is evident that the shape of the FT main peak is quite different for the 1 and 5 ppm data: the latter results in reduced

intensity and presents a double-peak shape. These effects are evidenced by the presence of Hg in the sample: it is clearly visible from the partial contributions in the k and R spaces that the AgM contribution and Ag_2Hg_3 result in phase opposition (see the orange line in Figure 3), attenuating the FT amplitude.

The quantitative analysis confirms a larger contribution of Ag−Hg coordination in the 5 ppm data; as can be seen in Table 1, the number of neighbors for the sample at 5 ppm ($N_{AgHg} = 1.2$) is approximately twice that of the sample at 1 ppm ($N_{AgHg} = 0.55$), while the FWHM is much larger for the 1 ppm sample.

The distances obtained appear very similar within the uncertainties in both samples for the Ag and Ag_2S phases, while the Ag−Hg coordination shells appear contracted in the 5 ppm sample with respect to the 1 ppm one. Although we must stress here that the uncertainty of the Ag−Hg coordination is quite large due to larger disorder and weaker contribution, this finding is in agreement with TEM findings that show a bimodal response of NP to Hg exposure: either Hg does not interact with Ag (so the pure Ag core remains unaffected) or the AgHg amalgam is formed in the whole NP volume.

The analysis of the Hg L_{III}-edge EXAFS data has been carried out considering contribution from both Ag_2Hg_3 and a Hg oxidized phase (HgO) to take into account an eventual Hg−O coordination. After some attempts, we found the Hg−O shell very weak (see Figure 4) and highly disordered (see
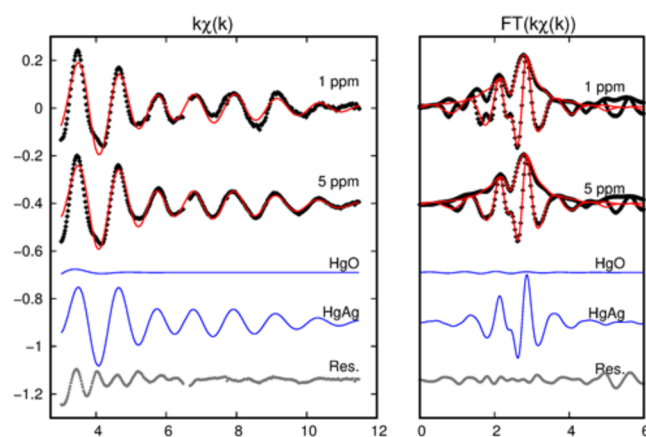
Figure 4. Hg L_{III}-edge results of AgNPs 1 and 5 ppm. Experimental (black dots) and fit (red curves) results are presented together with the contribution involved in the analysis shifted vertically for the sake of clarity. In the left panel, the fit is reported in the k space, while in the right panel, the Fourier transform is reported in the R space.

Table 2) even if this contribution statistically improves the quality of the refinement. We must notice that the weakness of the Hg−O signal and the correlation between σ^2 and N increases the incertitude of their values, but in accordance with XPS results, such a Hg−O shell suggests molecular

Table 1. Best Fit Results for Ag K-Edge XAFS Data Analysis of 1 and 5 ppm Samples

	AgM		Ag_2S		Ag_2Hg_3		
sample	R_{AgAg} (Å)	σ^2 (10^{-2} Å^2)	$R_{AgS}^{Ag_2S}$ (Å)	σ^2 (10^{-2} Å^2)	R_{AgHg} (Å)	σ^2 (10^{-2} Å^2)	N
1 ppm	2.857(5)	0.94(4)	2.44(2)	0.97(6)	2.97(8)	0.94(5)	0.55(5)
5 ppm	2.855(5)	0.92(3)	2.47(2)	1.9(2)	2.87(2)	0.26(3)	1.2(1)

Table 2. Best Fit Results for Hg L_{III}-Edge XAFS Data Analysis of 1 and 5 ppm Samples

sample	Hg−O			Ag$_2$Hg$_3$		
	R_{HgO_I} (Å)	σ^2 (10^{-2} Å^2)	N	R_{AgHg} (Å)	σ^2 (10^{-2} Å^2)	N
1 ppm	2.60(1)	5.0(4)	2.9(5)	2.87(2)	1.34(7)	9.7(7)
5 ppm	2.66(1)	9.2(5)	3.1(6)	2.89(2)	1.5(8)	12(1)

coordination compatible with the oxygen of the SO_3^- moiety. The k-weighted experimental spectra and best fits for the 1 ppm and 5 ppm spectra are reported in Figure 4 along with their Fourier transform.

The XAFS experimental data depict a higher noise with respect to the Ag K-edge spectra, the fit was performed in the k space from 3.0 to 11.5 Å^{-1} and required three contributions: the AgHg single scattering path at 2.9 Å from the Ag$_2$Hg$_3$ phase, which represents the larger fraction of the signal, and two very weak single scattering contributions, Ag−O$_I$ and Ag−O$_{II}$, expected from the Hg−O phase, respectively, at 2.6 and 2.7 Å. The structural parameters are shown in Table 2. Due to larger noise and the relatively short k-range of the analysis, the structural parameters from the Hg L_{III}-edge EXAFS spectra are affected by some larger uncertainty.

The analysis confirms the formation of an AgHg compound at a distance that agrees with the expected value of 2.9 Å. Shorter distances are obtained from a Hg−O contribution that improves the fit, but the Hg−O contributions are definitely weak with respect to the quite intense Hg−Ag signal, as seen in Figure 4.

Morphological Investigation. The TEM images of AgNP-3MPS before and after Hg(II) addition are shown in Figure 5a,b, respectively. AgNP-3MPS has a spherical shape in
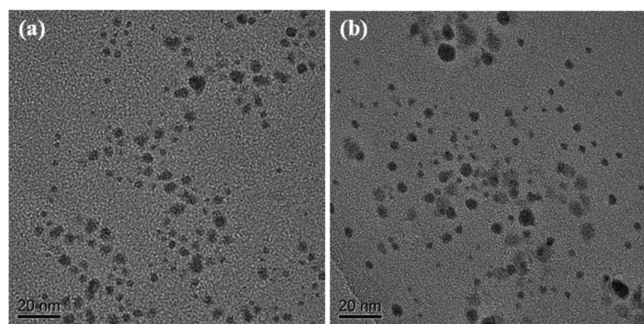

Figure 5. TEM images of AgNP-3MPS (a) before and (b) after Hg(II) addition at a concentration of 1 ppm.

both cases; thus, the presence of the pollutant does not affect the shape of the metal nanoparticles. The statistical analysis of 500 nanoparticles reveals a mean diameter of 3.71 ± 1.47 nm (the size dispersion graph is shown in Figure S3). In the case of AgNP-3MPS contaminated with 1 ppm of Hg(II), two different populations of NPs were found: the first one with a mean diameter of 3.53 ± 1.36 nm and the second with a mean diameter of 7.36 ± 1.50 nm (Figure S4a,b reports the size dispersion of both populations, respectively). Figure 6a,b shows the HAADF-STEM images of AgNP-3MPS and AgNP-3MPS/Hg(II), respectively, while Figure 6c,d represents the EDS maps (EDS spectra of AgNP-3MPS before and after interaction with Hg(II) are reported in Figure S6 in the Supporting Information). The STEM analysis coupled with the EDS map investigation highlighted important aspects. First of all, some NPs present bright parts with a high amount of Hg
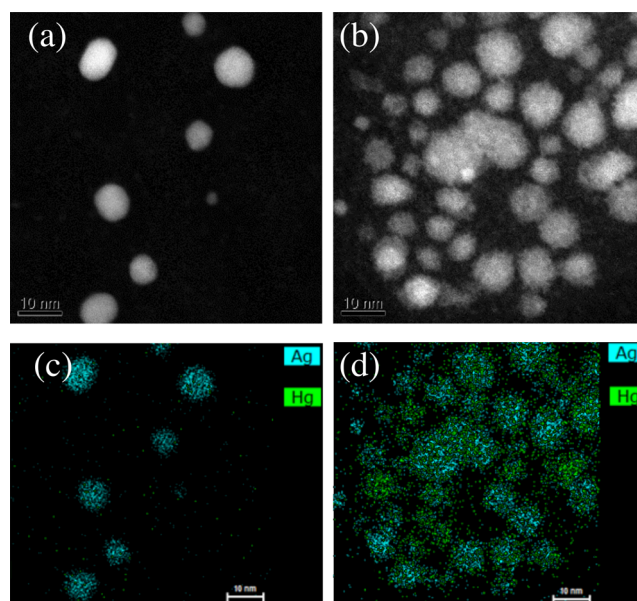

Figure 6. STEM images of AgNP-3MPS (a) before and (b) after Hg(II) addition at a concentration of 1 ppm and EDS maps of AgNP-3MPS (c) before and (d) after Hg(II). The scale bar is 10 nm in all images.

and a low porosity, while some others present dark regions with less Hg content and high porosity (see Figure S5a). Moreover, it is evident that a different distribution of Hg atoms occurs depending on the AgNP size. The smallest population has none or only a few Hg atoms interacting with the NPs; on the contrary, the bigger-sized particles have a uniform distribution of Hg atoms on their entire volume, forming a Ag/Hg amalgam and not a core−shell structure. The atomic composition as determined by semiquantitative EDS analysis of the Ag/Hg amalgam yields 66 and 34% for Ag and Hg, respectively (see Figure 6d). The HRTEM analysis suggests that Hg(II) ions interact preferentially with the larger particles at first, forming the Ag/Hg amalgam and leaving the smallest particles unmodified. This selective interaction could be related to a low structural defectivity of the small-sized NPs coupled with greater surface coverage by 3MPS with respect to the bigger ones. In fact, it is reported in the literature that a thick and stable coverage on the silver nanoparticle surface is protective toward Ag passivation, oxidation, and, therefore, for AgNPs exposed to Hg(II) and Ag−Hg interaction, giving rise to a Ag/Hg amalgam.[16,42]

Optical Characterization. The optical absorption spectra of AgNP-3MPS and AgNP-3MPS/Hg(II) at different concentrations are displayed in Figure 7a. The absorption spectrum of bare silver nanoparticles presents a localized surface plasmon resonance (LSPR) with a sharp and well-defined maximum at 399 nm, which was taken as the reference. On adding 1 ppm (red curve in the figure), the absorption band shifts to 385 nm. On increasing the content of contaminant in the colloidal solution, the blue shift increases even more, and for 5 ppm of
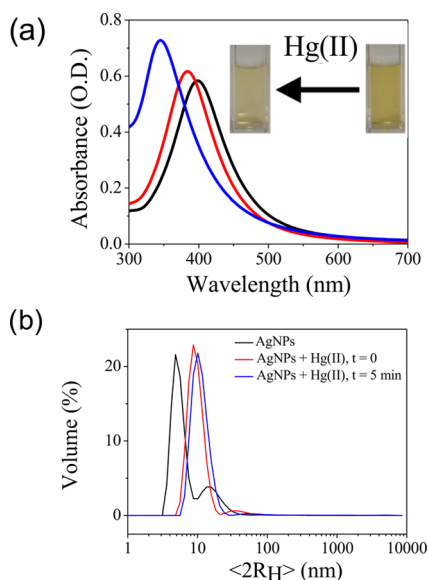
Figure 7. (a) Optical absorption of the AgNP solution with different concentrations of Hg(II). Black, red, and blue curves correspond to 0, 1, and 5 ppm, respectively; the inset shows the color change of the solution with 5 ppm of Hg(II). (b) DLS data in deionized water for pristine AgNP-3MPS (black curve) compared with the same sample exposed to 1 ppm Hg(II) solution (red curve at $t = 0$; blue curve after 5 min exposition).

Hg(II), the band maximum peaks at 348 nm (blue curve). According to our measurements (XPS, EXAFS, and TEM) and the literature,[43] the presence of Hg(II) seems to induce the formation of homogeneous nanoparticles of AgHg alloys. The observed blue shift can be related to the confinement of the electrons on the surface of the new AgHg alloy particles. Moreover, the increase in the background signal in the absorption spectra on increasing the amount of Hg indicates a large presence of big and heavy nanoparticles, which are the ones that interact with Hg(II) ions through the $-SO_3^-$ moieties (as also suggested by the Hg(II) contribution in the Hg 4f XPS spectra and the Hg−O shell revealed by XAFS). Such an optical behavior is accompanied by an evident change in color of the colloidal solution from yellow to yellowish/ colorless, as seen in the inset of Figure 7a. It has to be underlined that such a consistent change in the absorption band energy as a function of Hg(II) can be explored for efficient optical sensing for the determination of the presence of mercury ions in water in the 1−5 ppm range. From preliminary measurements, we found a sensitivity down to hundreds of ppb, but a more detailed characterization is currently under investigation.

The size and size distribution of AgNP-3MPS before and after interaction with Hg(II) solution were studied by DLS. Measurements evidenced a complex population on the pristine AgNPs with a dominant population with a hydrodynamic size distribution of colloidal samples equal to $<2R_H>$ 5 ± 2 nm and a secondary population with $<2R_H>$ 12 ± 4 nm (see Figure 7b). After interaction with 1 ppm Hg(II) solution, the size distribution highlights an increase in the hydrodynamic parameters with a size of $<2R_H>$ 10 ± 2 nm, quite stable with time. This outcome suggests that AgNP-3MPS undergoes rapid and stable aggregative phenomena after interaction with Hg(II) solution. The same result can be observed with a higher Hg(II) concentration (5 ppm; results shown in Figure S7 in

the Supporting Information). The increase in the hydro-dynamic radius upon interaction can be compared with UV−vis and TEM results confirming the aggregation and the change in the local dielectric constant around the nano-particles.

CONCLUSIONS

In this work, a multitechnique investigation of AgNPs stabilized by 3MPS molecules and interacting with Hg(II) ions was carried out, allowing us to gather information about the chemical composition, local atomic structure, and morphological behavior of the proposed system. SR-XPS analysis evidenced the partial reduction of Hg(II) ions to metallic Hg(0) and the overall stability of the 3MPS ligand. XAS data analysis pointed out the occurrence of a direct interaction between silver and mercury, thus suggesting a mixed AgNP−Ag/Hg alloy system; however, neither spectro-scopic technique is able to discern between the core−shell nanoparticles (for example, with a silver core and a Ag/Hg alloy shell, as often reported in the literature for analogous systems) and a mixture of pristine silver nanoparticles and newly formed alloy nanoparticles. TEM investigations shed light on this aspect, revealing the presence of two populations of spherical nanoparticles: pristine silver nanoparticles of small size (3.53 ± 1.36 nm) and newly formed Ag/Hg alloy nanoparticles of larger dimensions (7.36 ± 1.50 nm). This information is especially required to optimize the synthesis route to prepare nanomaterial-based sensors that provide simple, low-cost, and rapid tracking of heavy metals in real samples in the main framework of protection and preservation of aquatic ecosystems.

ASSOCIATED CONTENT

Ⓢ Supporting Information

The Supporting Information is available free of charge at https://pubs.acs.org/doi/10.1021/acs.jpcc.0c06951.

> C 1s and O 1s SR-XPS spectra of AgNP-3MPS + Hg 1 ppm and AgNP-3MPS + Hg 5 ppm (Figure S1a); C 1s, O 1s, and Hg 4f SR-XPS spectra of AgNP-3MPS + Hg 1 ppm and AgNP-3MPS + Hg 5 ppm and Ag 3d and S 2p SR-XPS spectra of AgNP-3MPS + Hg 1 ppm with the subtracted baselines reported in all spectra (Figure S1b); k^2-weighted EXAFS signal measured on 1 and 5 ppm samples (Figure S2); size dispersion of AgNP-3MPS (Figure S3); size dispersion of AgNP-3MPS polluted with 1 ppm of Hg(II) (Figure S4); AgNP-3MPS with 1 ppm of Hg(II): (a) STEM image and (b) EDS map (Figure S5); EDS spectra of AgNP-3MPS with Hg(II): (a) selected areas, (b) bright field, and (c) dark field (Figure S6); and DLS data in deionized water for pristine AgNP-3MPS compared with AgNP-3MPS exposed to 5 ppm Hg(II) solution (Figure S7) (PDF)

AUTHOR INFORMATION

Corresponding Author

Chiara Battocchio − *Department of Sciences, Roma Tre University of Rome, 00146 Rome, Italy;* ⓞ orcid.org/0000-0003-4590-0865; Email: chiara.battocchio@uniroma3.it

Authors

Irene Schiesaro − *Department of Sciences, Roma Tre University of Rome, 00146 Rome, Italy*

Luca Burratti − *Department of Industrial Engineering and INSTM, University of Rome Tor Vergata, 00133 Rome, Italy*

Carlo Meneghini − *Department of Sciences, Roma Tre University of Rome, 00146 Rome, Italy;* orcid.org/0000-0003-4846-8422

Ilaria Fratoddi − *Department of Chemistry, Sapienza University of Rome, 00185 Rome, Italy;* orcid.org/0000-0002-5172-0636

Paolo Prosposito − *Department of Industrial Engineering and INSTM, University of Rome Tor Vergata, 00133 Rome, Italy*

Joohyun Lim − *Department of Chemistry, Kangwon National University, Chuncheon 24341, Republic of Korea;* orcid.org/0000-0003-3880-2634

Christina Scheu − *Max-Planck-Institut für Eisenforschung GmbH, 40237 Düsseldorf, Germany;* orcid.org/0000-0001-7916-1533

Iole Venditti − *Department of Sciences, Roma Tre University of Rome, 00146 Rome, Italy;* orcid.org/0000-0002-9306-573X

Giovanna Iucci − *Department of Sciences, Roma Tre University of Rome, 00146 Rome, Italy;* orcid.org/0000-0002-6478-3759

Complete contact information is available at:
https://pubs.acs.org/10.1021/acs.jpcc.0c06951

Author Contributions

[$]The manuscript was written through the contributions of all authors. All authors have given approval to the final version of the manuscript. I.S. and L.B. contributed equally.

Notes

The authors declare no competing financial interest.

ACKNOWLEDGMENTS

ABBREVIATIONS USED

SR, synchrotron radiation; SR-XPS, synchrotron radiation-induced X-ray photoelectron spectroscopy; XAS, X-ray absorption spectroscopy; XANES, X-ray absorption near-edge spectroscopy; TEM, transmission electron microscopy; DLS, dynamic light scattering

REFERENCES

(1) Islam, M. S.; Ahmed, M. K.; Habibullah-Al-Mamun, M. Heavy Metals in Cereals and Pulses: Health Implications in Bangladesh. *J. Agric. Food Chem.* **2014**, *62*, 10828−10835.

(2) Fu, J.; Zhang, A.; Wang, T.; Qu, G.; Shao, J.; Yuan, B.; Wang, Y.; Jiang, G. Influence of E-Waste Dismantling and Its Regulations: Temporal Trend, Spatial Distribution of Heavy Metals in Rice Grains, and Its Potential Health Risk. *Environ. Sci. Technol.* **2013**, *47*, 7437−7445.

(3) Rahman, M. T.; Kabir, M. F.; Gurung, A.; Reza, K. M.; Pathak, R.; Ghimire, N.; Baride, A.; Wang, Z.; Kumar, M.; Qiao, Q. Graphene Oxide−Silver Nanowire Nanocomposites for Enhanced Sensing of Hg2+. *ACS Appl. Nano Mater.* **2019**, *2*, 4842−4851.

(4) Waheed, A.; Mansha, M.; Ullah, N. Nanomaterials-Based Electrochemical Detection of Heavy Metals in Water: Current Status, Challenges and Future Direction. *Trends Anal. Chem.* **2018**, *105*, 37−51.

(5) Yang, Z.; Liu, H.; Li, J.; Yang, K.; Zhang, Z.; Chen, F.; Wang, B. High-Throughput Metal Trap: Sulfhydryl-Functionalized Wood Membrane Stacks for Rapid and Highly Efficient Heavy Metal Ion Removal. *ACS Appl. Mater. Interfaces* **2020**, *12*, 15002−15011.

(6) Ciotta, E.; Paoloni, S.; Richetta, M.; Prosposito, P.; Tagliatesta, P.; Lorecchio, C.; Venditti, I.; Fratoddi, I.; Ciardi, S.; Pizzoferrato, R. Sensitivity to Heavy-Metal Ions of Open-Cage Fullerene Quantum Dots. *Sensors* **2017**, *17*, 2614.

(7) Galashev, A. Y. Modeling of Forced Desorption Processes in a Regenerable Graphene Sorbent for Elemental Mercury Capture. *J. Phys. Chem. C* **2016**, *120*, 13263−13274.

(8) Maiti, S.; Barman, Ga.; Laha, J. K. Detection of Heavy Metals (Cu+2, Hg+2) by Biosynthesized Silver Nanoparticles. *Appl. Nanosci.* **2016**, *6*, 529−538.

(9) Schopf, C.; Wahl, A.; Martín, A.; O'Riordan, A.; Iacopino, D. Direct Observation of Mercury Amalgamation on Individual Gold Nanorods Using Spectroelectrochemistry. *J. Phys. Chem. C* **2016**, *120*, 19295−19301.

(10) Ackerman, A. H.; Creed, P. A.; Parks, A. N.; Fricke, M. W.; Schwegel, C. A.; Creed, J. T.; Heitkemper, D. T.; Vela, N. P. Comparison of a Chemical and Enzymatic Extraction of Arsenic from Rice and an Assessment of the Arsenic Absorption from Contaminated Water by Cooked Rice. *Environ. Sci. Technol.* **2005**, *39*, 5241−5246.

(11) Jian, J.; Chen, W. Graphene Quantum Dots as a Fluorescence Probes for Sensing Metal Ions: Synthesis and Applications. *Curr. Org. Chem.* **2015**, *19*, 1150−1162.

(12) Ravindran, A.; Elavarasi, M.; Prathna, T. C.; Raichur, A. M.; Chandrasekaran, N.; Mukherjee, A. Selective Colorimetric Detection of Nanomolar Cr (VI) in Aqueous Solutions Using Unmodified Silver Nanoparticles. *Sens. Actuators, B Chem.* **2012**, *166*, 365−371.

(13) Liu, J.; Vellaisamy, K.; Yang, G.; Leung, C.-H.; Ma, D.-L. Luminescent Turn-On Detection of Hg(II) Via the Quenching of an Iridium(III) Complex by Hg(II)-Mediated Silver Nanoparticles. *Sci. Rep.* **2017**, *7*, No. 3620.

(14) Prosposito, P.; Burratti, L.; Venditti, I. Silver Nanoparticles as Colorimetric Sensors for Water Pollutants. *Chemosensors* **2020**, *8*, 26.

(15) Bootharaju, M. S.; Praedeep, T. J. Uptake of Toxic Metal Ions from Water by Naked and Monolayer Protected Silver Nanoparticles: An X-ray Photoelectron Spectroscopic Investigation. *J. Phys. Chem. C* **2010**, *114*, 8328−8336.

(16) Prosposito, P.; Burratti, L.; Bellingeri, A.; Protano, G.; Faleri, C.; Corsi, I.; Battocchio, C.; Iucci, G.; Tortora, L.; Secchi, V.; Franchi, S.; Venditti, I. Bifunctionalized Silver Nanoparticles as Hg^{2+} Plasmonic Sensor in Water: Synthesis, Characterizations, and Ecosafety. *Nanomaterials* **2019**, *9*, 1353.

(17) Ding, Y.; Wang, S.; Lib, J.; Chen, L. Nanomaterial-Based Optical Sensors for Mercury Ions. *Trends Analyt. Chem.* **2016**, *82*, 175−190.

(18) Lou, T.; Chen, Z.; Wang, Y.; Chen, L. Blue-to-Red Colorimetric Sensing Strategy for Hg2+ and Ag+ via Redox-Regulated Surface Chemistry of Gold Nanoparticles. *ACS Appl. Mater. Interfaces* **2011**, *3*, 1568−1573.

(19) Chen, L.; Li, J.; Chen, L. Colorimetric Detection of Mercury Species Based on Functionalized Gold Nanoparticles. *ACS Appl. Mater. Interfaces* **2014**, *6*, 15897−15904.

(20) Ling, L.; Fu, X.; Lu, W.; Chen, L. Highly Sensitive and Selective Colorimetric Sensing of Hg2+ Based on the Morphology Transition of Silver Nanoprisms. *ACS Appl. Mater. Interfaces* **2013**, *5*, 284−290.

(21) Boruah, B. S.; Daimari, N. K.; Biswas, R. Functionalized Silver Nanoparticles as an Effective Medium Towards Trace, Determination of Arsenic (III) in Aqueous Solution. *Results Phys.* **2019**, *12*, 2061−2065.

(22) Paul, D.; Dutta, S.; Saha, D.; Biswas, R. LSPR Based Ultra-Sensitive Low-Cost U-Bent Optical Fiber for Volatile Liquid Sensing. *Sens. Actuators, B* **2017**, *250*, 198−207.

(23) Mochi, F.; Burratti, L.; Fratoddi, I.; Venditti, I.; Battocchio, C.; Carlini, L.; Iucci, G.; Casalboni, M.; De Matteis, F.; Casciardi, S.; Nappini, S.; Pis, I.; Prosposito, P. Plasmonic Sensor Based on Interaction between Silver Nanoparticles and Ni2+ or Co2+ in Water. *Nanomaterials* **2018**, *8*, 488.

(24) Corsi, P.; Venditti, I.; Battocchio, C.; Meneghini, C.; Bruni, F.; Prosposito, P.; Mochi, F.; Capone, B. Designing an Optimal Ion Adsorber at the Nanoscale: The Unusual Nucleation of AgNP/Co^{2+}−Ni^{2+} Binary Mixtures. *J. Phys. Chem. C* **2019**, *123*, 3855−3860.

(25) Bootharaju, M. S.; Chaudhari, K.; Praedeep, T. Real Time Plasmonic Spectroscopy of the Interaction of Hg^{2+} with Single Noble Metal Nanoparticles. *RSC Adv.* **2012**, *2*, 10048−10056.

(26) Schiesaro, I.; Battocchio, C.; Venditti, I.; Prosposito, P.; Burratti, L.; Centomo, P.; Meneghini, C. Structural Characterization of 3d Metal Adsorbed AgNPs. *Phys. E* **2020**, *123*, No. 114162.

(27) Battocchio, C.; Meneghini, C.; Fratoddi, I.; Venditti, I.; Russo, M. V.; Aquilanti, G.; Maurizio, C.; Bondino, F.; Matassa, R.; Rossi, M.; Mobilio, S.; Polzonetti, G. *J. Phys. Chem. C* **2012**, *116*, 19571−19577.

(28) Prosposito, P.; Mochi, F.; Ciotta, E.; Casalboni, M.; Matteis, F. D.; Venditti, I.; Fontana, L.; Testa, G.; Fratoddi, I. Hydrophilic Silver Nanoparticles with Tunable Optical Properties: Application for the Detection of Heavy Metals in Water. *Beilstein J. Nanotechnol.* **2016**, *7*, 1654−1661.

(29) Moulder, J. F.; Stickle, W. F.; Sobol, P. E.; Bomben, K. D. *Handbook of X-ray Photoelectron Spectroscopy*; Prairie, E., Eds.; Physical Electronics Inc.: Minnesota, 1996.

(30) Beamson, G.; Briggs, D. *High Resolution XPS of Organic Polymers, The Scienta ESCA 300 Database*; John Wiley & Sons: Chichester, 1992.

(31) Di Cicco, A.; Aquilanti, G.; Minicucci, M.; Principi, E.; Novello, N.; Cognigni, A.; Olivi, L. Novel Xafs Capabilities at Elettra Synchrotron Light Source. *J. Phys.: Conf. Ser.* **2009**, *190*, No. 012043.

(32) Meneghini, C.; Bardelli, F.; Mobilio, S. Estra-Fitexa: a Software Package for Exafs Data Analysis. *Nucl. Instrum. Methods Phys. Res., Sect. B* **2012**, *285*, 153−157.

(33) Rehr, J. J.; Albers, R. C. Theoretical Approaches to X-Ray Absorption Fine Structure. *Rev. Mod. Phys.* **2000**, *72*, 621.

(34) Ankudinov, A. L.; Ravel, B.; Rehr, J.; Conradson, S. D. Real-Space Multiple-Scattering Calculation and Interpretation of X-Ray-Absorption Near-Edge Structure. *Phys. Rev. B* **1998**, *58*, 7565.

(35) Carlini, L.; Fasolato, C.; Postorino, P.; Fratoddi, I.; Venditti, I.; Testa, G.; Battocchio, C. Comparison between Silver and Gold Nanoparticles Stabilized with Negatively Charged Hydrophilic Thiols: SR-XPS and SERS as Probes for Structural Differences and Similarities. *Collo. Surf. A* **2017**, *532*, 183−188.

(36) Marchioni, M.; Battocchio, C.; Joly, Y.; Gateau, Ch.; Nappini, S.; Pis, I.; Delangle, P.; Michaud-Soret, I.; Deniaud, A.; Veronesi, G. Thiolate-Capped Silver Nanoparticles: Discerning Direct Grafting from Sulfidation at the Metal−Ligand Interface by Interrogating the Sulfur Atom. *J. Phys. Chem. C* **2020**, *124*, 13467−13478.

(37) Sun, T. S.; Buchner, S. P.; Byer, N. E. Oxide and Interface Properties of Anodic Films on Hg1−xCdxTe. *J. Vac. Sci. Technol.* **1980**, *17*, 1067.

(38) NIST. *X-ray Photoelectron Spectroscopy Database, Version 4.1*; National Institute of Standards and Technology: Gaithersburg, 2012.

(39) Manivannan, S.; Seo, Y.; Kang, D.-K.; Kim, K. Colorimetric and Optical Hg(II) Ion Sensor Developed with Conjugates of M13-Bacteriophage and Silver Nanoparticles. *New J. Chem.* **2018**, *42*, 20007−20014.

(40) Manivannan, S.; Ramaraj, R. Silver Nanoparticles Embedded in Cyclodextrin−Silicate Composite and their Applications in Hg(ii) Ion and Nitrobenzene Sensing. *Analyst* **2013**, *138*, 1733−1739.

(41) Turner, M.; Vaughan, O. P. H.; Kyriakou, G.; Watson, D. J.; Schrerer, L. J.; Davidson, G. J. E.; Sanders, J. K. M.; Lambert, R. M. Deprotection, Tethering, and Activation of a One-Legged Metal-loporphyrin on a Chemically Active Metal Surface: NEXAFS, Synchrotron XPS, and STM Study of [SAc]P-Mn(III)Cl on Ag(100). *J. Am. Chem. Soc.* **2009**, *131*, 1910−1914.

(42) Marchioni, M.; Gallon, T.; Worms, I.; Jouneau, P.-H.; Lebrun, C.; Veronesi, G.; Truffier-Boutry, D.; Mintz, E.; Delangle, P.; Deniaud, A.; Michaud-Soret, I. Insights into Polythiol-Assisted AgNP Dissolution Induced by Bio-Relevant Molecules. *Environ. Sci.: Nano* **2018**, *5*, 1911−1920.

(43) Bhattacharjee, Y.; Amarnath, C. Label-free Cysteamine-Capped Silver Nanoparticle-based Colorimetric Assay for Hg (II) Detection in Water with Subnanomolar Exactitude. *ACS Sustain. Chem. Eng.* **2014**, *2*, 2149−2154.